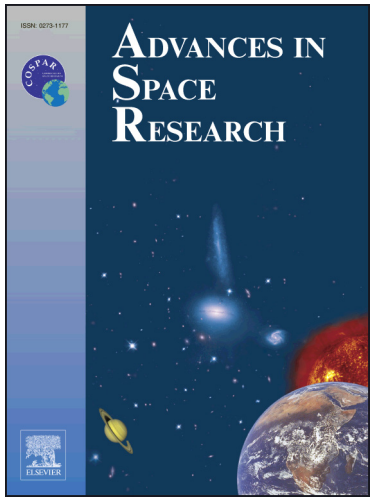


# Study of Ionospheric Scintillation Characteristics in Australia with GNSS during 2011-2015

Kai Guo, Yan Zhao, Yang Liu, Jinling Wang, Chunxi Zhang, Yanbo Zhu

PII: S0273-1177(17)30180-1
DOI: http://dx.doi.org/10.1016/j.asr.2017.03.007
Reference: JASR 13141

To appear in: *Advances in Space Research*

Received Date: 22 April 2016
Revised Date: 4 March 2017
Accepted Date: 8 March 2017

Please cite this article as: Guo, K., Zhao, Y., Liu, Y., Wang, J., Zhang, C., Zhu, Y., Study of Ionospheric Scintillation Characteristics in Australia with GNSS during 2011-2015, *Advances in Space Research* (2017), doi: http://dx.doi.org/10.1016/j.asr.2017.03.007

# Study of Ionospheric Scintillation Characteristics in Australia with GNSS during 2011-2015

Kai Guo[a], Yan Zhao[a], Yang Liu[a,d]*,

Jinling Wang[b], Chunxi Zhang[a], Yanbo Zhu[c]

[a]*School of Instrumental Science and Opto-Electronics Engineering, Beihang University, Beijing 100191, P.R.China*

[b]*School of Civil and Environmental Engineering, University of New South Wales, Sydney, NSW 2052, Australia*

[c]*School of Electronic Information and Engineering, Beihang University, Beijing 100191, P.R.China*

[d] *Collaborative Innovation Center for Geospatial Information Technology , No.129 Luoyu Road ,Wuhan, 430079,P.R.China*

## Abstract

Ionospheric scintillation has a great impact on radio propagation and electronic system performance, thus is extensively studied currently. The influence of ionospheric scintillation on Global Navigation Satellite System (GNSS) is particularly evident, making GNSS an effective method to study characteristics of scintillation. In this paper, spatial-temporal statistical features of ionospheric scintillation are intensively studied based on GNSS scintillation data provided by Space Weather Service (SWS) in Australia. Most scintillation data are measured by observation stations in Australia region during 2011 to 2015. A data processing and analyzing framework is proposed to investigate scintillation features in this paper. General pictures of amplitude scintillation activities observed at different stations are first explored. It is found that scintillation activity presents a manifest seasonal variation at most stations during the researched time spans. The probabilities of amplitude scintillation of different intensities are also evaluated. In the experiment to investigate signal amplitude distributions, Nakagami-m and α-μ distribution models are applied to describe the measured amplitude distribution curves. The result shows that the α-μ model provides a more approximate description for the measured distributions. Kurtosis and information entropy are also calculated to further verify this conclusion. The proposed study is of great significance for a better understanding of ionospheric scintillation in the region of Australia, and for discovering the effects of scintillation on GNSS signals.

*Keywords:* ionospheric scintillation, Nakagami-m, α-μ distribution, scintillation intensity

*Corresponding author. Tel.: +86 10 82316547 823

E-mail address: liuyangee@buaa.edu.cn (Y. Liu).

# 1. Introduction

Ionosphere is an ionized region in the earth's upper atmosphere where the molecules can be decomposed into ions and electrons under the radiation of the sun, affecting the propagation of radio frequency waves. Most often, the main effect of the active ionosphere on GNSS is a range delay to the signal, for the speed and direction are changed when the signal passes though the turbulent plasmas. This delay leads to a measurement error for the navigation positioning solution (Jin et al., 2008, 2011, 2016b). Currently, ionospheric delay errors have been widely researched and can be mitigated by dual frequency mechanism(Jin et al., 2014, 2015, 2016a). However, the inhomogeneity of the electron density in the ionosphere affects the signal quality as well, which is still a complex problem and not yet resolved.

When radio frequency signal transmits through the ionospheric irregularities, the amplitude and phase are likely to suffer an intense fluctuation, called ionospheric scintillation(Fremouw et al., 1978). It has been researched that the scintillation is closely associated with the solar and geomagnetic activities, and presents geographical and seasonal distribution characteristics(Abdu et al., 1998, Basu and Basu, 1981).

Typically, ionospheric scintillation can be divided into amplitude and phase scintillations. Amplitude scintillation is usually more frequent and intense in equatorial regions, while phase scintillation is likely to appear at high latitudes (Basu et al., 1988). It occurs mainly during the sunset and early morning hours, and peaks at equinoxes during a year (Tam Dao and Vinh Duong, 2013).

The major effects of ionospheric scintillation on GNSS can be considered in two aspects (Kintner et al., 2007, Conker et al., 2003, Elmas et al., 2011, Humphreys et al., 2010). Firstly, it probably causes a sharp decrease in amplitude intensity leading to cycle slips, even a complete unlock to satellite signals. Secondly, the phase could suffer from a rapid fluctuation which results in an increase of tracking loop errors. Thus, the performance of GNSS receiver and positioning accuracy may decrease in the presence of scintillations. However, the influenced signal conversely provides a medium for measuring and modeling the ionospheric scintillation phenomenon. Although scintillation is hard to predict, a comprehensive analysis is helpful to better understand it.

Extensive studies have been carried out on ionospheric scintillations. Researchers(Chen et al., 2008) have analyzed characteristics of GNSS observations under ionospheric scintillation during solar maximum years from 2001 to 2003. Similarly the effects of ionospheric scintillation on GNSS have also been studied in Brazil under solar maximum years from 2012 to 2013(Fortes et al., 2015). Researchers in Stanford University also investigate aviation GNSS performance under ionospheric scintillation(Conker et al., 2003), and these studies keep under intense focus. Researchers further investigate the links between GNSS signal scintillation and calibrated total electron content (TEC) gradients during solar maximum, in which TEC spatial gradients is found to be larger during equinoctial seasons(Cesaroni et al., 2015). However, those studies focus too much on the data during solar maximum, while other spans of time has been ignored. To thoroughly investigate the ionospheric scintillation effects on GNSS signal and its performance, further studies are conducted based on more comprehensive data. Data of 2008-2013 included a deep solar minimum and the rising phase toward solar maximum are well investigated to analyze phase scintillation characteristics in polar region, which reveals the close relationship between geographical factors and the scintillation occurrence(Prikryl et al., 2015). In addition, C/NOFS data are used to study the plasma bubble occurrence and its strong link with scintillation in low and middle solar activity years(Huang et al.,

2014). Researchers(Akala et al., 2014) analyzed scintillation data over Logos, Nigeria on daily, monthly and seasonal time scales during the minimum and ascending phases (2009-2011) of solar cycle 24. Other limitation of previous studies lies on the fact that regional properties of ionospheric scintillation are under minor investigation. While previous data are only collected with one geographical feature, near equatorial region or near the pole, those data have no counterparts to discuss ionospheric scintillation behaviors. Thus the spatial and temporal characteristics of ionospheric scintillation cannot be discussed in a general picture. Yu Jiao(Jiao et al., 2014) conducted a comprehensive analysis of the scintillation data collected from observation stations Alaska and Jicamarca respectively, but the data spans of the two stations are not equal, thus no obvious contrast effect is confirmed.

To address the problems above, spatial-temporal statistical characteristic of ionospheric scintillation in Australia region is discussed in this paper. The study is based on the data sets provided by SWS in Australia from 2011 to 2015. These data sets are collected and selected by strict criteria to form a reliable data pool for further investigation. Based on the numerous data, this work aims at contributing to a better understanding of the scintillation characteristics in the region of Australia. In order to accomplish this task, a statistical analysis model is established to evaluate the different behaviors of scintillation. The characteristics of amplitude scintillation measured by monitor stations are discussed, which is one of the key points in this research. General pictures of the amplitude scintillation over all the research time spans at different monitor stations are demonstrated and a comparison of the amplitude scintillation occurrence rates between stations is also made. Then the probability density functions (PDFs) of amplitude scintillation index are evaluated. With the PDFs acquired, the probabilities of amplitude scintillation of different strengths can be calculated directly.

Another key points in this paper is the statistical analysis of the signal amplitude distribution under the scintillation. The PDF distribution curves are compared with theoretical Nakagami-m and α-μ distribution models through the implementation of variance analysis. Then kurtosis and information entropy are introduced here to further illustrate and verify the characteristics of the signal amplitude distribution under the effect of scintillation.

The rest of this paper is organized as follows: Section 2 involves a brief description of the distribution models and statistical methods, as a baseline theory for the proposed study. In Section 3, the proposed method for data analysis and statistical algorithm are discussed at length, which demonstrates the idea of this work. Section 4 is related to the discussion of characteristics of amplitude scintillation based on the data sets preprocessed in Section 3. At last, the conclusions of this study are given in Section 5.

# 2. Baseline theory

## *2.1 Ionospheric Scintillation*

Ionospheric scintillation is a kind of phenomenon that the signal amplitude or phase suffer a rapid and random fluctuations when signals pass through the ionosphere. The inhomogeneity and irregularity of ionic clusters determine the scintillation intensity directly. Ionospheric scintillation can be divided into amplitude and phase scintillation. To quantify the scintillation intensity, and analyze the characteristic of scintillation, the indices $S_4$ and $\sigma_\phi$ are introduced in this paper. $S_4$ index indicates the intensity of amplitude scintillation and it is defined as the normalized root mean square (*RMS*) of the received signal power (Knight, 2000, Aquino et al., 2007, Crisci et al., 2001):

$$S_4 = \sqrt{\frac{\langle I^2 \rangle - \langle I \rangle^2}{\langle I \rangle^2}} \tag{1}$$

where $I = R^2$ is the intensity of signal and $R$ is amplitude of the received signal; $\langle \cdot \rangle$ denotes time average. In this study, the features of amplitude scintillation are mainly researched.

$\sigma_\phi$ index represents the phase scintillation intensity and is defined as the normalized *RMS* of the received signal phase, given by(Jiao et al., 2014, Aquino et al., 2007):

$$\sigma_\phi = \sqrt{\langle \phi^2 \rangle - \langle \phi \rangle^2} \tag{2}$$

where $\phi$ is the detrended phase of signal.

Different thresholds are used to classify the scintillation in researches. Considering that scintillation with $S_4$ lower than 0.3 is relative weak and contributes little to the study of ionosphere GNSS signals(Aquino et al., 2009, Humphreys et al., 2010), threshold of $S_4$ = 0.3 is used to define the minimum scintillation researched in this paper. Based on the amplitude scintillation index, we divide the scintillation into four intensity levels in this paper, as shown in Table.1.

Table.1 Ionospheric scintillation intensity classified by $S_4$ index

| *$S_4$ index* | *Scintillation Intensity* |
|---|---|
| < 0.3 | very weak |
| 0.3 ~ 0.5 | weak |
| 0.5 ~ 0.7 | moderate |
| ≥ 0.7 | strong |

## *2.2 The Nakagami-m distribution*

Signal fading channels have been extensively investigated for long and many models are employed to describe the attenuation signal (Nunes and Sousa, 2014, Wernik et al., 2007, Yeh and Liu, 1982), contributing to a better understanding of the signal distribution under scintillation. Nakagami-m PDF was one of the most popular and approximate functions to describe the distribution of signal amplitude in scintillation environment (de Oliveira Moraes et al., 2013, Fremouw et al., 1978). The Nakagami-m PDF is defined as:

$$f_R(r) = \frac{2m^m r^{2m-1}}{\Gamma(m)\Omega^m} e^{-mr^2/\Omega} \tag{3}$$

where $r$ is a single element of vector $R$ and $\Gamma(\cdot)$ denotes Gamma function given by:

$$\Gamma(x) = \int_0^{+\infty} t^{x-1} e^{-t} \mathrm{d}t, \quad x > 0 \tag{4}$$

$$\Gamma(x) = (x-1)!, \quad = 1, 2 \tag{5}$$

where $m$ indicates the degree of attenuation and is calculated by $m = 1/(S_4)^2$; $\Omega = E\{r^2\}$ is the average of signal power. When the signal amplitude is normalized ($\Omega = E\{r^2\} = 1$), Eq.(3) can be rewritten as (de Oliveira Moraes et al., 2013):

$$f_R(r) = \frac{2m^m r^{2m-1}}{\Gamma(m)} e^{-mr^2} \tag{6}$$

### *2.3 The α-μ distribution*

Yacoub (Yacoub, 2007) proposed a Gamma based distribution model, α-μ distribution, which assumes that the signal is a combination of clusters of multipath waves. The α-μ distribution has one more degree of freedom, making it much more adaptable to describe the amplitude distribution curves, in particular for tails. It has been validated that the α-μ distribution can provide a more realistic and accurate approximate to the signal amplitude distribution under scintillation. For normalized amplitude, α-μ distribution are given by(de Oliveira Moraes et al., 2013):

$$f_R(r)=\frac{\alpha r^{\alpha\mu-1}}{\xi^{\alpha\mu/2}\Gamma(\mu)}\exp\left(-\frac{r^{\alpha}}{\xi^{\alpha/2}}\right),\quad \xi=\frac{\Gamma(\mu)}{\Gamma(\mu+2/\alpha)} \tag{7}$$

where α and μ are two parameters which can be estimated based on the equation:

$$\frac{E^2\left(R^{\beta}\right)}{E\left(R^{2\beta}\right)-E^2\left(R^{\beta}\right)}=\frac{\Gamma(\mu)\Gamma(\mu+4/\alpha)-\Gamma^2(\mu+2/\alpha)}{\Gamma^2(\mu+2/\alpha)} \tag{8}$$

It should be noted that the α parameter may change considerably even for the same $S_4$ value. A lager α usually indicates a stronger fading intensity. Meanwhile, the Nakagami-m model is a particular case of α-μ distribution model when α = 2 and μ = *m*. For more details about α-μ distribution model, readers may refer to (Oliveira Moraes et al., 2014). In this paper, both Nakagami-m and α-μ distribution are employed to describe the signal distribution under amplitude scintillation.

# 3. The proposed method

### *3.1 Parzen Window Method*

Frequency histogram method is a common method to estimate the PDF of sample, however, the main drawback is that the estimated density function is not smooth enough, and the estimated result is considerably affected by the group distance. As a result, Parzen window method (Babich and Camps, 1996) is employed in this work. Parzen window method, also known as kernel density estimation, is often used to estimate the PDF of an unknown sequence in mathematical statistic and data mining theory, which is a kind of non-parametric test methods. In this paper, Parzen window method is applied to estimate the PDF of scintillation of different intensities and the distribution of amplitude under the interference of scintillation. Parzen window method is described as follows:

Assuming that the sample $X=\{x_1, x_2, \ldots, x_n\}$ agrees with an unknown PDF in the *D* dimensional space, then the probability in the region *R* is given by:

$$P=\int_R p(x)\mathrm{d}x \tag{9}$$

where $p(x)$ is the PDF and *P* is the probability that each sample point falls into region *R*. Then we employed *k* to represent the number of sample point that falls into region *R*, in the case of *n* is large enough and region *R* is small enough, the equation above can be rewritten as

$$p(x)\approx\frac{k}{n\cdot V} \tag{10}$$

where *V* is the volume contained in the area *R*. By defining window function as

$$H(u)=\begin{cases} 1, & |u|\le \frac{1}{2} \\ 0, & otherwise \end{cases} \tag{11}$$

$k$ can be calculated as:

$$k_n=\sum_{i=1}^{n} H\left(\frac{x-x_i}{h_n}\right) \tag{12}$$

where $h_n$ is the length of $R$ region. Combining Eq.(7) to Eq.(10), the PDF is given by:

$$p_n(x)=\frac{1}{nh}\sum_{i=1}^{n} H\left(\frac{x-x_i}{h}\right) \tag{13}$$

In this study, Gaussian function was employed as the window function.

## *3.2 Residual analysis and variance analysis*

Residual and variance are analyzed to statistically evaluate the difference between measured distribution and theoretical distribution. The baseline theory comes from mathematical statistics, where residual and variance analysis are often employed to evaluate the significance of PDF fitting and PDF regression. The indicators used in this paper are listed as follows.

(1)*RMSE*: the root mean of square error, defined as:

$$RMSE=\sqrt{\frac{1}{n}\sum_{i=1}^{n}\left(y_i-\hat{y}_i\right)^2} \tag{14}$$

where $y_i$ is observed value and $\hat{y}_i$ is the corresponding estimated value.

(2)*R-square*: the coefficient of determination, which implies how well the data fit a statistical model. It is given by:

$$R-square=1-\frac{SSE}{SST} \tag{15}$$

where *SST* is total sum of squares and defined as:

$$SST=\sum_{i=1}^{n}\left(y_i-\overline{y}_i\right)^2 \tag{16}$$

*SSE* is the sum of square error, defined as:

$$SSE=\sum_{i=1}^{n}\left(y_i-\hat{y}_i\right)^2 \tag{17}$$

$\overline{y}_i$ is the arithmetic mean of sample data. It can be known that the *R-squared* ranges from 0 to 1. Generally, the more the indicator is close to 1, the better the regression curve fits the sample data. In this paper, both *RMSE* and *R-square* are adapted to indicate how close the theoretical distributions can approximate the measured curves.

## *3.3 Kurtosis and information entropy*

To comprehensively illustrate the outline of PDF curves as well as the non-Gaussian property, kurtosis is introduced in this paper, which is a classical measure reflecting the shape of curves. The normal distribution is employed as the standard to determine the thickness of tails for certain PDF. A larger kurtosis implies curves with thicker tails and wider ranges. For a stochastic variable $X$ with fourth-order moment existed, the kurtosis is given by:

$$C_k = \frac{E(X - E(X))^4}{[E(X - E(X))^2]^2} - 3 \tag{18}$$

Kurtosis is closely related with high order statistical parameter and indicates the non-Gaussian and non-linearity for certain PDF. Here we use kurtosis to investigate the property of signal amplitude distribution under different levels of scintillation. However, as discussed previously, multipath also has a strong interference in GNSS signal amplitude. To further discuss the characteristic of scintillation, a criterion should be introduced to distinguish between strong scintillation and strong multipath under given amplitude scintillation index. Here information entropy is used to meet with such demand. Information entropy is first applied in information theory to measure the order of information, meanwhile reflect the amount of information. A higher information entropy indicates a more disordered system. The extent of randomness and uncertainty of the system is quantified by calculating information entropy. For a discrete symbol sets, information entropy $H$ is given by

$$H = -\sum_{i=1}^{m} P_i \log_2 P_i \tag{19}$$

where $P_i$ is the probability of $v_i$. Additionally, when $P$=0, the equation above is invalid. Since ionospheric scintillation presents great randomness and uncertainty, the information entropy is applied to describe the distribution of amplitude under scintillation. In the paper, the differences between measured probability density distribution and theoretical probability density distribution are compared by calculation and analysis of kurtosis and information entropy.

### *3.4 Overall procedures*

The main issues in this study mainly contain (i) discussing the characteristics of amplitude scintillation observed at Australia regions and (ii) analyzing the distribution of amplitude under scintillation. Based on the methods above the overall process is proposed, as shown in Fig.1. There are four main steps in the whole process.

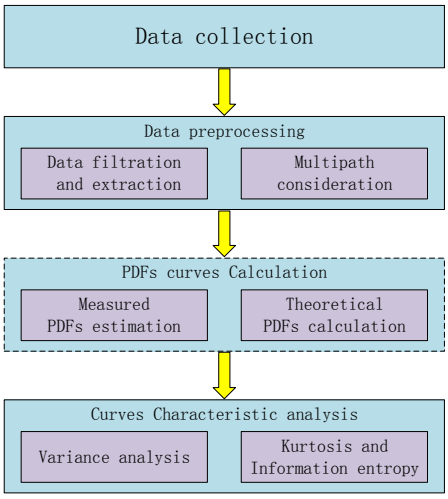


Fig.1 The overall process of the research

*Step 1: Data collection*

In this paper, data of the monitor stations located at different latitudes are selected to investigate ionospheric scintillation characteristics in Australia. The locations and observation-time spans of each station are listed in Table.2. The data sets contain plenty of scintillation data with a recording period of 1 minute, which makes the study more persuasive and acceptable. It should be noted that as the scintillation data sets at Vanimo stations are not available during 2011 to 2015, only scintillation observations from 2007 to 2009 at this station are selected in this paper, and the results are processed separately as a contrast with other results.

Table.2 Locations and observation-time spans at different monitor stations

| *Station* | *Time span* | *Latitude (°S)* | *Longitude (°E)* | *Geomagnetic Latitude (°S)* | *Geomagnetic Longitude (°E)* |
|---|---|---|---|---|---|
| *Vanimo* | 2007~2009 | 2.70 | 141.30 | 11.19 | 212.90 |
| *Darwin* | 2011~2015 | 12.45 | 130.95 | 21.96 | 202.84 |
| *Weipa* | 2011~2015 | 12.63 | 141.88 | 21.79 | 214.41 |
| *Niue* | 2013~2015 | 19.07 | 190.07 | 20.84 | 265.42 |
| *Macquarie Island* | 2011~2015 | 54.50 | 158.95 | 64.54 | 248.10 |

Global Positioning System Ionospheric Scintillation Monitors (GPS ISMs) are employed by International Planetarium Society (IPS) for the observations. These ISMs are built around NovAtel OEM GPS receiver cards and specially modified to improve the tracking performance. Therefore, the receiver can maintain locked to satellite even under strong scintillation. GPS ISMs can output 50Hz high frequency scintillation data. Unfortunately, the SWS only provides processed data recorded every 1 minute in the daily scintillation data files. Meanwhile, the $S_4$ index analyzed in this paper has been corrected with the internal receiver noise removed. Because the signal amplitude is not contained in the data files directly, L1 Carrier to Noise Ratio (*L1 CN*0) acted as an indicator of amplitude in the analysis. It should be mentioned that since a different type of monitoring receiver might be employed at Vanimo and the scintillation data is available only for a solar minima period, the results obtained at this station are presented separately as a comparison with those obtained at other stations.

*Step 2: Data preprocessing*

Usually there are 9 parameters recorded in the scintillation data files. Due to the rather large amount of data, some errors and outliers were encountered when $S_4$ index was extracted from data files. To make

the scintillation data more accurate and effective, we applied a data purification procedure to detect and exclude the errors and outliers. As for the focus of the research is the characteristic of scintillation, we will not go into details of the error excluding and outlier detecting. Additionally, in the presence of multipath, the divergence of signal amplitude is faster, and the scintillation observations can also be contaminated (Aquino et al., 2009). GNSS data observed at elevations lower than 30° is therefore filtered out in this paper. By this way, most of the multipath can be avoided.

*Step 3: Probability density function calculation*

The PDF of a certain observed measurements can be roughly obtained through frequency histogram method. However, the estimated density function is not smooth enough, and the estimated result is considerably affected by the group distance in frequency histogram. Therefore, Parzen window method is adopted to calculate PDFs for a higher accuracy and more deterministic descriptions in this step. After the measured curves are estimated, the theoretical ones are also calculated.

*Step 4: Statistical characteristic analysis*

In the study of amplitude distribution under scintillation, variance analysis method is firstly applied to quantify the deviation between theoretical PDF curves and measured caves. To verify the result of variance analysis as well as evaluate how the theoretical can describe the measured distributions, kurtosis and the information entropy are computed to analyze the curves more comprehensively.

In order to make the research more efficient, a Graphical User Interface (GUI) is implemented, as demonstrated in Fig.2. All the steps are combined in this GUI, and the results of analysis can be directly shown after data processing and calculation.

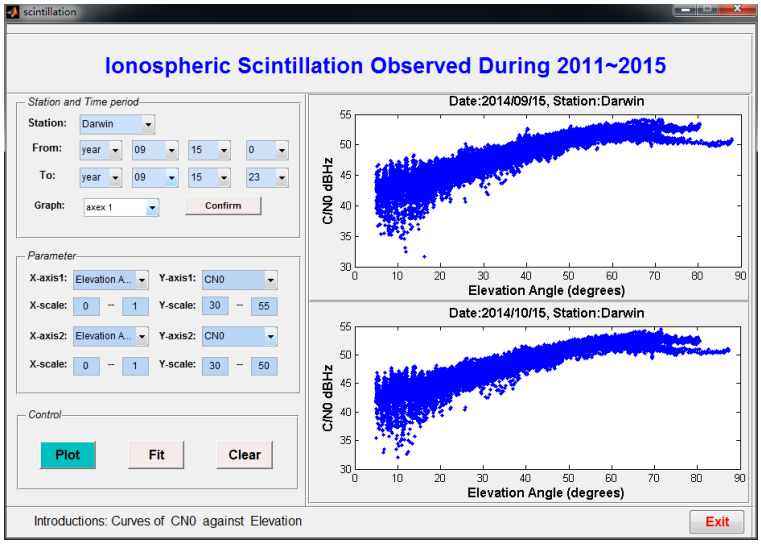


Fig.2 The GUI developed in the proposed work

# 4. Characteristics of Scintillation

## *4.1 General pictures of amplitude scintillation activities*

In this section, an overall statistical result for the amplitude scintillation measured at different stations is first explored. Results show that there is a noticeable seasonal fluctuation during the researched time spans at most stations, that is to say the peaks are more likely to concentrate at equinoxes and the valleys probably appear in summer and winter. Fig.3 displays the variation of amplitude scintillation frequency presented in Vanimo, Darwin and Macquarie Island stations, which are typical examples of

observatories in low, middle and high latitudes respectively. The seasonal variation is not verified at Vanimo. This is because the scintillation frequency at this station maintains high for almost all the months. Besides, the amplitude scintillation frequency at Vanimo surpasses others significantly even during the valley of the solar cycle year from 2007 to 2009, which implies that scintillation in equatorial zone is much more active than other zones, and latitude factors have more effects on ionospheric scintillation than solar activity.

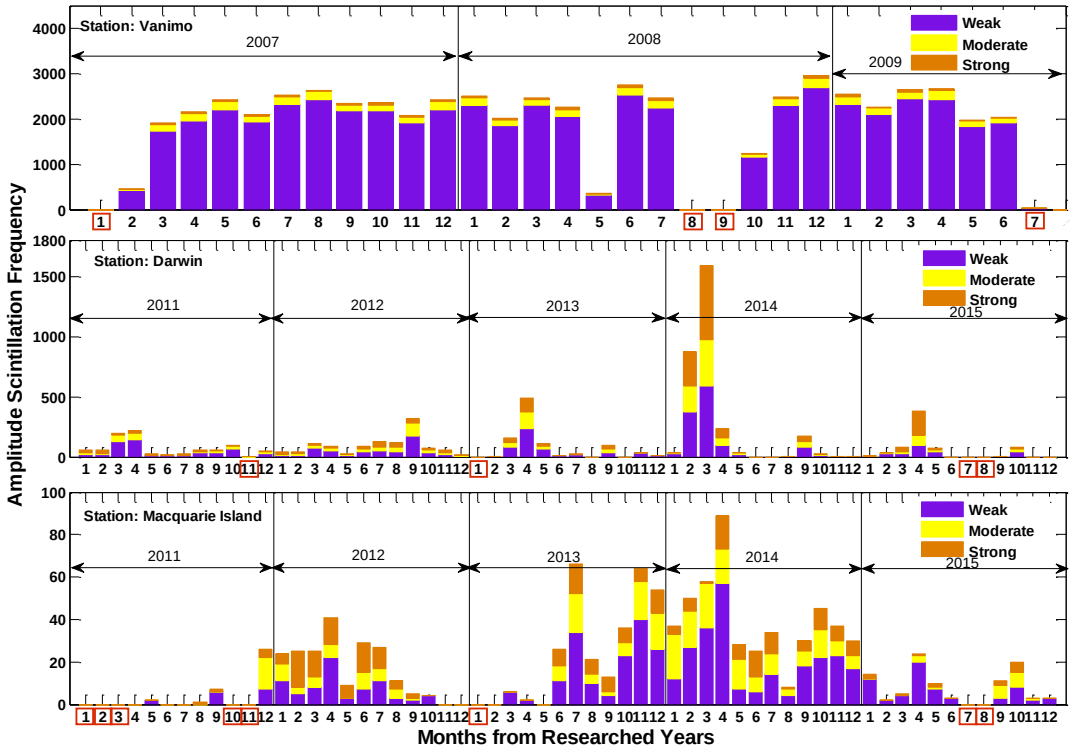


Fig.3 Seasonal amplitude scintillation variations observed at Vanimo, Darwin and Macquarie Island stations respectively (The month label in red square indicates that the available scintillation data files are less than 3 days in that month)

In addition, the amplitude scintillation dramatically increased around March and April 2014 over most stations. This outstanding ascent is in accordance with the variation of solar activity in solar cycle 24 which started from the minimum in year 2009 and reached maximum on April 2014, as shown in Fig.4. It is apparent that the solar activity is relative low before 2010, and increases gradually from 2011 and peaks at 2014.

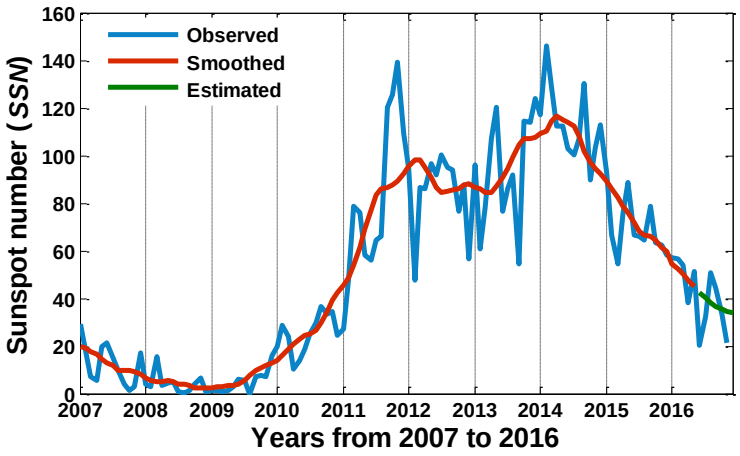

Fig.4 The variation of *SSN* from 2007 to 2016

Another experiment was implemented to identify the difference of scintillation occurrence rates caused by geographical distribution of the sites. In this experiment, occurrence rates of amplitude scintillation during all the research time spans were calculated. Fig.5 reveals the results of station Niue, Darwin, Weipa and Macquarie Island, the geomagnetic latitudes of which elevate generally. The calculation results of Vanimo were not presented in the figure, because the scintillation occurrence rate in Vanimo is extremely high, almost over one hundred times than that in other stations. Besides, the researched time spans at this station are not align with others and the solar activity varies largely. As it is shown in the figure, the amplitude scintillation occurrence rates decline gradually with the growth of latitude and reach the minimum in Macquarie Island, which agrees with the previous researches that amplitude scintillation in equatorial zone and middle latitudes is more active than that in high latitude areas.

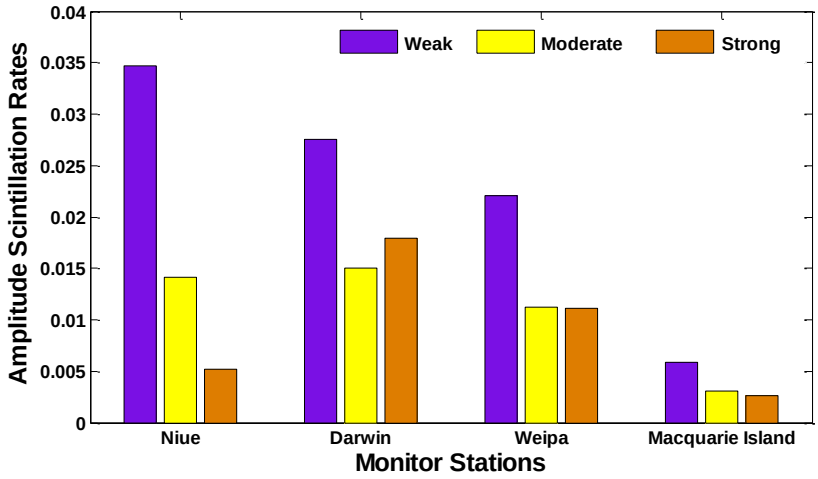


Fig.5 Comparison of amplitude scintillation rates calculated at Niue, Darwin, Weipa and Macquarie Island stations during 2011-2015

The results may attribute to the different geophysical conditions in the researched stations. For instance, the solar flux in equatorial zone is weaker than that in mid-latitudes, which may result in the different scintillation characteristics between Vanimo and stations located in mid-latitudes. Additionally, the solar and geomagnetic field activity also influence the scintillation intensity and frequency. Details of how geophysical factors and solar and geomagnetic field activity influence the ionospheric scintillation are out of the range of this paper and will be focused in the follow-on researches.

## *4.2 Statistics of Amplitude Scintillation Intensity*

Amplitude scintillation indicator $S_4$ is widely adopted to indicate the intensity of ionospheric scintillation. In this section, a comprehensive study is conducted to explore the $S_4$ distributions at different stations. It should be noted that only scintillation with $S_4 \geq 0.3$ is counted in this analysis. As shown in Table.4, the total numbers of extracted scintillations with elevation > 30° at each station are listed in the second row. The next two rows are the frequencies and probabilities of amplitude scintillation captured by ISMs. According to Table.3, there are more scintillations observed at middle latitude stations, which is consistent with geographical distribution characteristics of amplitude scintillations discussed in the previous section.

Table.3 Ionospheric amplitude scintillation probabilities at different monitoring stations

| *Station* | *Darwin* | *Weipa* | *Niue* | *Macquarie* |
|---|---|---|---|---|

| | | | | *Island* |
|---|---|---|---|---|
| *scintillation with elevation>30°* | 10835643 | 10633864 | 5114983 | 9490139 |
| *amplitude scintillation with* $S_4 \geqslant 0.3$ | 6551 | 4730 | 2759 | 1090 |
| $P_{occur}$ (%) | 0.0605 | 0.0445 | 0.0539 | 0.0115 |

Based on the calculated probabilities of amplitude scintillation with $S_4 \geq 0.3$, another experiment is implemented to evaluate the PDF curves by Parzen window method. A three-parameter power function is then employed to fit the curve. The function is given by

$$p(S_4) = a \times (S_4)^b + c \tag{18}$$

where *a, b, c* are three independent parameters. The fitting results are listed in Table.4. According to the columns of *R-square* and *RMSE*, it is clear that the power function agrees well with the curves.

Table.4 Fitting results of the distribution curves of $S_4$ at different stations

| *Stations* | *a* | *b* | *c* | *R-square* | *RMSE* |
|---|---|---|---|---|---|
| *Darwin* | 0.2023 | -2.226 | 0.6173 | 0.9289 | 0.1890 |
| *Weipa* | 0.3625 | -1.9 | 0.2904 | 0.9220 | 0.2382 |
| *Niue* | 0.8801 | -1.663 | -0.8566 | 0.9929 | 0.1162 |
| *Macquarie Island* | 0.1818 | -2.567 | 0.4881 | 0.8699 | 0.3559 |

To make a more intuitive comparison among different stations and provide a spatial behavior of ionospheric scintillation in Australia, the $S_4$ PDF curves are plotted based on the parameters in Table.4. As shown in Fig.6, The PDF curve of Niue is much higher than other stations when $S_4$ is lower than approximately 0.6, indicating that weak scintillation is more likely to occur in this stations. This conclusion agrees with the results demonstrated in Fig.5 in the previous section.

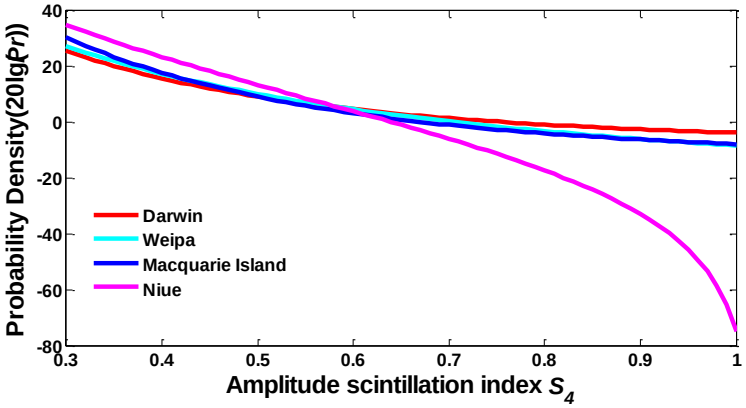


Fig.6 PDF curves of amplitude scintillation index $S_4$ at different observation stations

With the PDFs acquired, the probabilities of amplitude scintillation of different strengths can be calculated directly. Since the PDFs are obtained in the condition of $S_4 \geq 0.3$, the probability here is a kind of conditional probability, as shown in Eq. (19):

$$P_{S_4} = P\{P(S_4) \mid P_{occur}\} = P_{occur} \times \int_{S_4-\Delta/2}^{S_4+\Delta/2} p(\Delta) \bullet \mathrm{d}\Delta \tag{19}$$

where $\Delta$ is the integration interval.

## *4.3 Statistics of Signal Amplitude under Amplitude Scintillation*

It has been mentioned that the signal amplitude can suffer a sharp decline in the presence of scintillation. As an example, Fig.7 illustrates the variation of *CN*0 values along with $S_4$ for PRN 19 and PRN 23 on March 9, 2014 at Darwin station. It can be seen that the values of *CN*0 fade apparently under the severe scintillations. In addition, there is a strong correlation between $S_4$ and *CN*0.

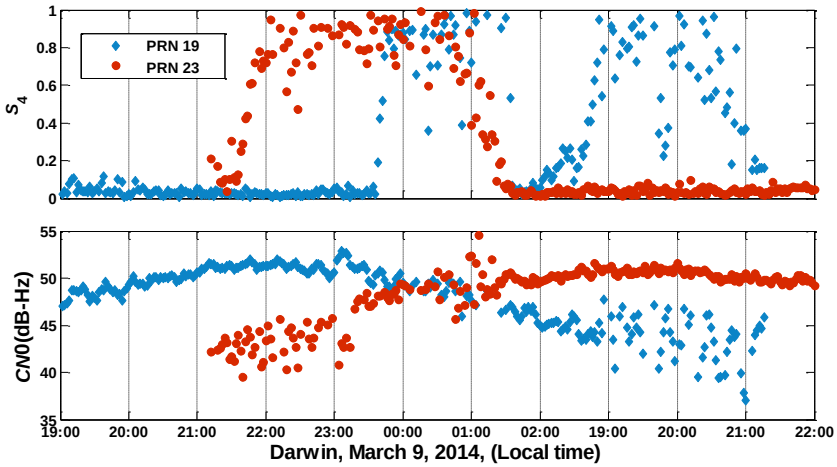


Fig.7 The *CN*0 values along with $S_4$ for PRN 19 and 23 on March 9, 2014 at Darwin station

The distribution of GPS signal amplitude under scintillation is another key point in this paper. In this research, *CN*0 is selected where $S_4$ varies from 0.3±0.05 to 0.9±0.05 by step of 0.1. Due to the fact that the amplitude scintillation occurred at Macquarie Island is relative inactive. In order to make the research more meaningful, only scintillation data from station Darwin, Weipa, Niue are processed and analyzed here. The numbers of scintillation samples for every $S_4$ index at different stations are shown in Table.5.

Table.5 Scintillation samples used in relation to monitor stations and $S_4$

| *Station* | $S_4$=*0.3* | $S_4$=*0.4* | $S_4$=*0.5* | $S_4$=*0.6* | $S_4$=*0.7* | $S_4$=*0.8* | $S_4$=*0.9* |
|---|---|---|---|---|---|---|---|
| *Darwin* | 2298 | 1413 | 1031 | 812 | 674 | 686 | 681 |
| *Weipa* | 1843 | 1173 | 697 | 629 | 457 | 402 | 469 |
| *Niue* | 1421 | 850 | 542 | 363 | 208 | 108 | 42 |

Based on the normalized *CN*0, the PDF is evaluated through Parzen window method. Then the measured curves, evaluated curves and theoretical curves are plotted together to make a comparison. Fig.8 reveals the results obtained at Darwin and Weipa station as typically examples. It can be seen from the figure that the evaluated curves are much smoother than the curves obtained directly from the scintillation data. Additionally, both theoretical Nakagami-m and α-μ distribution models provide good descriptions to the evaluated curves correspondingly. Furthermore, *RMSEs* between measured and theoretical Nakagami-m (*RMSE1*) and α-μ (*RMSE2*) distributions are also marked in the figure.

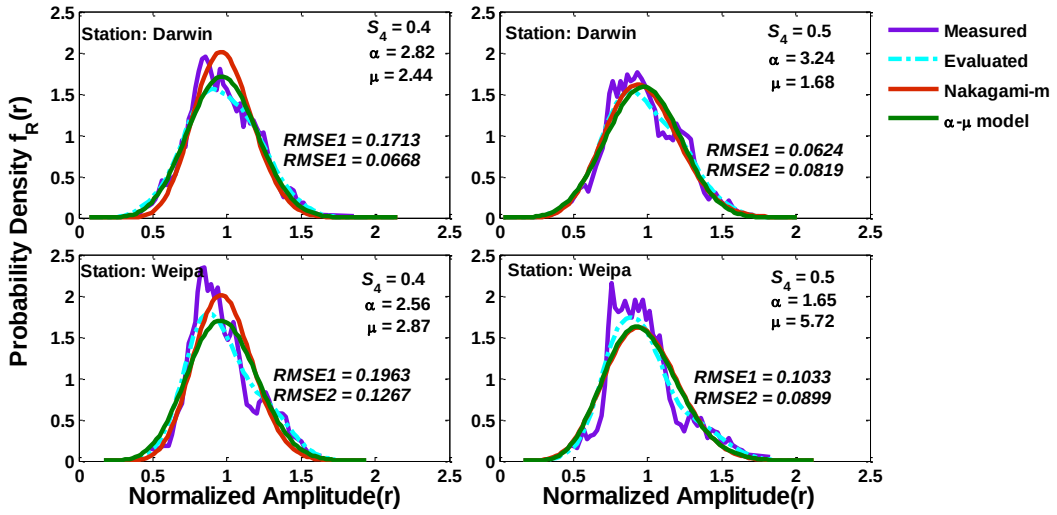


Fig.8 Probability density distribution curves of normalized amplitude in relation to $S_4$ index at Darwin and Weipa station

Table.6 lists the evaluated parameter α of α-μ distribution model at Darwin, Weipa and Niue stations. It can be seen from the table that α values at Niue are relative high, which means that the fading intensity at this station is stronger. Additionally, compared with the α values evaluated based on the scintillation data collected at São José dos Campos (23.1°S; 45.8°W; dip latitude 17.3°S) between December 2001 and January 2002 (de Oliveira Moraes et al., 2013, Oliveira Moraes et al., 2014), the α values in this research are still higher as a whole, even if the solar activity during 2011 to 2015 is not as intense as that during 2001 to 2002. This result may result from the special locations of the stations where the intensity of ionospheric scintillation is relative serious. As a result, it can be concluded the influences of latitudes or locations are more than that of solar activity on ionospheric scintillation.

Table.6 The evaluated parameter α in relation to monitor stations and $S_4$

| *Station* | $S_4$=0.3 | $S_4$=0.4 | $S_4$=0.5 | $S_4$=0.6 | $S_4$=0.7 | $S_4$=0.8 | $S_4$=0.9 |
|---|---|---|---|---|---|---|---|
| *Darwin* | 2.99 | 2.82 | 3.24 | 1.45 | 1.38 | 1.28 | 2.06 |
| *Weipa* | 3.11 | 2.56 | 1.65 | 0.44 | 1.24 | 1.86 | 1.84 |
| *Niue* | 3.82 | 2.30 | 4.46 | 4.16 | 3.74 | 3.86 | 3.38 |

To further evaluate the performances of Nakagami-m and α-μ distributions when they are used to describe the amplitude distributions under scintillation, the *RMSEs* between evaluated and theoretical distributions (both Nakagami-m and α-μ distributions) are calculated at different stations respectively. The *RMSE*s at certain $S_4$ values which vary from 0.3 to 0.9 measured at Darwin, Weipa and Niue stations are displayed in Fig.9.

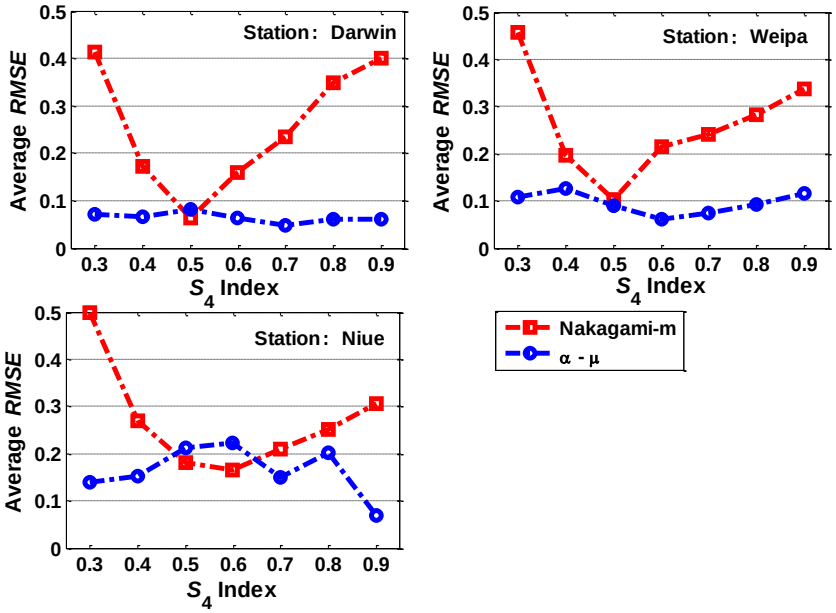


Fig.9 *RMSEs* in relation to $S_4$ index at Darwin, Weipa and Niue stations

As shown in the figure, when $S_4$ is lower than 0.5 the *RMSE* curves for Nakagami-m distribution decreases gradually as $S_4$ increases at all the stations. The downward trend slows down and *RMSE* approaches the lowest points when $S_4$ is around 0.5, indicating that the Nakagami-m distribution can approximate the scintillation better when the intensity is moderate. As for the uptrend of *RMSEs* when $S_4 > 0.5$, it is possible due to the assumption of single layer model of ionosphere is conditional, especially when the ionosphere is quiet. Thus under strong scintillations, Nakagami-m distribution for amplitude scintillation may be no longer suitable. On the other hand, compared with Nakagami-m distribution, the *RMSE* curves for α-μ distribution maintain at a lower level which implies that the signal amplitude distribution under scintillation can be better described by α-μ distribution.

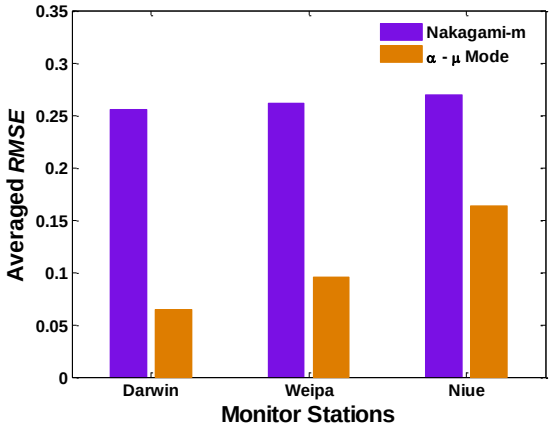


Fig.10 Averaged *RMSEs* at Darwin, Weipa and Niue stations

The average *RMSE*s at these stations are also calculated, as Fig.10 demonstrates. It is evident that the average *RMSEs* for Nakagami-m distribution are greatly higher than that of α-μ model over all the stations, indicating that the theoretical α-μ model PDFs preforms better when describing the amplitude distribution under scintillation. Additionally, *RMSEs* vary dramatically between stations. This might due to the considerable scintillation intensity and frequency differences between these stations. In addition, the *RMSEs* at Niue station is relative high than the other stations, which is likely result from

that the data sets are fewer because only scintillation data from 2011 to 2013 are processed at this station.

Kurtosis and information entropy are then introduced here to further illustrate how the theoretical distributions describe the measured distribution of amplitude, as well as to investigate features of the measured distribution curves. Kurtosis is a classical measure reflecting the dispensability of the curve tail. A larger kurtosis usually implies a curve with thicker tails and a wider range. In this experiment, the kurtosis coefficients for measured distribution curves and theoretical distribution curves are calculated respectively. With the offsets between kurtosis of different curves obtained by applying subtraction operation, the offsets are averaged for each $S_4$ value at Darwin, Weipa and Niue stations.

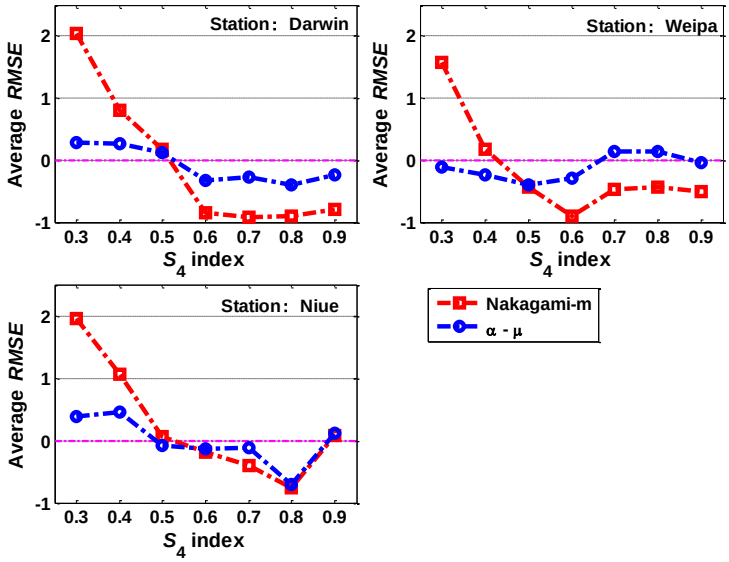


Fig.11 Offset of kurtosis in relation to $S_4$ at Darwin, Weipa and Niue stations

Fig.11 unfolds the kurtosis offsets for Nakagami-m and α-μ distributions at stations Darwin, Weipa and Niue. As the figure shows, when $S_4$ is lower than 0.6, the kurtosis offsets at these three stations between measured and Nakagami-m distributions decline with the increase of $S_4$, which signifies that **the tails of measured distribution are closer to Nakagami-m with the increase of $S_4$**. This result agrees with the conclusion drawn from Fig.9 that the distribution of amplitude under moderate scintillation would be better approximated by Nakagami-m distribution. By contrast, the kurtosis offsets between measured and α-μ distributions are much smaller, almost around 0, indicating that this model is better at describing the tail of the curves. This result embodies the superiority of α-μ distribution by applying two parameters instead of only one when fitting signal amplitude. When $S_4$ surpasses around 0.5, the lines for α-μ model remain low, except for station Niue, at which the lines share a similar tendency. This trend implies that Nakagami-m and α-μ model perform similarly for modeling amplitude under moderate and strong scintillation at this station.

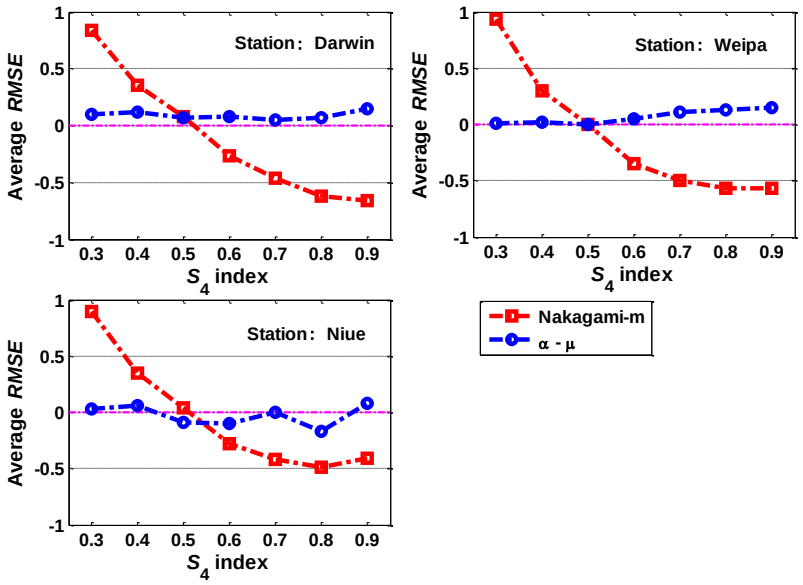


Fig.12 Deviation of information entropy in relation to $S_4$ at Darwin, Weipa and Niue stations

Information entropy is a criterion to evaluate the randomness and uncertainty of a specific sequence. In this paper the indicator is adopted to represent the complexity of the distribution curves. The deviation of information entropy between measured and theoretical distribution curves for $S_4$ value at Darwin, Weipa, and Niue stations are calculated to quantify the complexity distinction among different curves. The averaged information entropy deviations are exhibited in Fig.12. As we can see the information entropy deviation between measured and Nakagami-m distribution decreases gradually with the growth of $S_4$ at these stations. The higher deviation appears when $S_4 = 0.3$, where the intensity of amplitude scintillation is relatively weak. In this case, the measured *CN*0 sequence are more random. When amplitude scintillation becomes stronger, the deviation approaches zero and remains at a relative low level, showing that the measured distribution matches the theoretical distribution approximately. On the other hand, the information entropy deviation between measured and α-μ distributions keeps low over all the $S_4$ value at Darwin, Weipa, and Niue, manifesting that the α-μ distribution curves have an approximate randomness and uncertainty with measured distributions.

Based on the analysis above, it can be concluded that both Nakagami-m and α-μ distributions can provide an approximation for the *CN*0 distribution curves under scintillation, however, α-μ distribution performs better. It is worth mentioning that the characteristics of ionospheric scintillations observed at **Darwin and Weipa are extremely similar**, which may result from the close geographically relationships between these two stations. The correlations of the scintillations deserve a further study. The result in this section is quite helpful for the researchers who are interested in the signal fading channel modeling. Additionally, the conclusion can be considered in the design of GNSS receivers, as well as the navigation and positioning solution process.

# 5. Concluding Remarks

In this paper spatial-temporal behaviors of ionospheric scintillation in Australia are investigated with the data sets provided by SWS from 2011 to 2015. This study aims at studying the ionospheric scintillation characteristics and researching the statistics of GPS signal amplitude under the effect of scintillation. As the signal amplitude and scintillation observations can be severely contaminated by

multipath, GNSS data measured at elevations lower than 30° is filtered out to minimum the effect of multipath interference in this study.

One of the key points in this paper is discussing the characteristics of amplitude scintillation measured by several monitor stations which are located at various latitudes. It is shown that the ionospheric scintillation measured by most stations follows seasonal variations. The peaks probably occur at the Spring Equinox and the Autumnal Equinox, while the valley bottoms are likely to take place during summer and winter. The occurrence rates of amplitude scintillation during the research time spans are also calculated. There is a gradually decrease of the amplitude scintillation rates with the growth of latitude, which agrees with the previous conclusion that the amplitude scintillations in equatorial and middle latitude zones are more active than that in high latitude areas.

To further verify the probabilities of $S_4$, a statistical analysis is implemented. A polynomial fitting function is employed with parameters distinguished by stations to model the PDF curves. With the PDF evaluated, the amplitude scintillation probabilities of different intensities can be obtained directly, which is meaningful for scintillation prediction and GNSS receiver design. The occurrence rates of amplitude scintillation and PDFs of $S_4$ at these stations are also compared, providing a spatial behavior of ionospheric scintillation in Australia.

Another key point in this paper is the research of signal amplitude distributions under amplitude scintillation. *CN*0 observations are employed in the study. The *RMSE*s between measured and theoretical distributions for $S_4$ values at Darwin, Weipa and Niue stations are calculated. Compared with Nakagami-m distribution, signal amplitude distributions can be better described by α-μ distribution, especially for weak scintillations. The averaged *RMSE*s at different stations are also calculated. They vary dramatically at different stations, which may due to the significant difference of scintillation intensity and frequency between stations.

In addition, kurtosis and information entropy are adopted here to describe the dispensability of the curve tails and the randomness of amplitude distribution in accordance with the intensity of scintillation. It can be seen that the kurtosis offsets between measured and α-μ distribution are much smaller at these three stations, almost around 0, indicating that this model is better at describing the tail of the curves. Additionally, the information entropy deviations between measured and Nakagami-m decrease with the growth of $S_4$, implying that there exists lager randomness difference between measured and Nakagami-m distribution curves for weak and strong scintillation. While the information entropy deviations between α-μ and measured distributions keep low, manifesting that this model has an approximate randomness and uncertainty with the measured distribution. The features of scintillation observed at Darwin and Weipa have a lot in common, which may result from the close geographically relationships between these two stations and deserves a further study.

In brief, the general characteristics of scintillation in Australia are thoroughly discussed in this paper. By applying a statistical analysis, a comprehensive understanding of scintillation in Australia space region is formed. Some of the scintillation features obtained in this work deserve further study. The future work will focus on spatial-temporal characteristics on specific monitor stations with general conclusions produced by this paper. Additionally, the relationships between the scintillation of different intensities and relevant factors, such as solar and geomagnetic field activity, can also be considered as the key issues for further discussion.

# Acknowledgments

This work was supported by the National Key Research and Development Plan by Ministry of Science and Technology (2016YFC1402502), National Natural Science Foundation of China under grant (61233005), (61301087), and National 973 Project under Grant (2014CB744200). The author would like to thank the reviewers for their detailed and insightful comments and constructive suggestions. Their valuable contributions helped the authors improve the quality of this work. Special thanks should be given to the Space Weather Service Bureau of Meteorology Australia for providing scintillation data for research.

# References

Abdu, M. A., Sobral, J. H. A., Batista, I. S., Rios, V. H. & Medina, C. 1998. Equatorial spread-F occurrence statistics in the American longitudes: Diurnal, seasonal and solar cycle variations. *Advances in Space Research,* 22(6)**,** 851-854.

Akala, A. O., Amaeshi, L. L. N., Doherty, P. H., Groves, K. M., Carrano, C. S., Bridgwood, C. T., Seemala, G. K. & Somoye, E. O. 2014. Characterization of GNSS scintillations over Lagos, Nigeria during the minimum and ascending phases (2009–2011) of solar cycle 24. *Advances in Space Research,* 53(1)**,** 37–47.

Aquino, M., Andreotti, M., Dodson, A. & Strangeways, H. 2007. On the use of ionospheric scintillation indices as input to receiver tracking models. *Advances in Space Research,* 40(3)**,** 426-435.

Aquino, M., Monico, J., Dodson, A. H., Marques, H., De Franceschi, G., Alfonsi, L., Romano, V. & Andreotti, M. 2009. Improving the GNSS positioning stochastic model in the presence of ionospheric scintillation. *Journal of Geodesy,* 83(10)**,** 953-966.

Babich, G. A. & Camps, O. I. 1996. Weighted Parzen windows for pattern classification. *Pattern Analysis and Machine Intelligence, IEEE Transactions on,* 18(5)**,** 567-570.

Basu, S. & Basu, S. 1981. Equatorial scintillations—a review. *Journal of Atmospheric & Terrestrial Physics,* 43(5-6)**,** 473-489.

Basu, S., Mackenzie, E. & Basu, S. 1988. Ionospheric constraints on VHF/UHF communications links during solar maximum and minimum periods. *Radio Science,* 23(03)**,** 363-378.

Cesaroni, C., Spogli, L., Alfonsi, L., De Franceschi, G., Ciraolo, L., Joao, F. G. M., Scotto, C., Romano, V., Aquino, M. & Bougard, B. 2015. L-band scintillations and calibrated total electron content gradients over Brazil during the last solar maximum. *Journal of Space Weather & Space Climate,* 5, A36.

Chen, W., Gao, S., Hu, C., Chen, Y. & Ding, X. 2008. Effects of ionospheric disturbances on GPS observation in low latitude area. *GPS Solutions,* 12(1)**,** 33-41.

Conker, R. S., El Arini, M. B., Hegarty, C. J. & Hsiao, T. 2003. Modeling the effects of ionospheric scintillation on GPS/Satellite‐Based Augmentation System availability. *Radio Science,* 38(1), 1001.

Crisci, M., Lannelongue, S., Guichon, H. & Martin, N. Optimisation of Galileo GRC Receivers in Ionospheric Scintillation Conditions. *Proceedings of the 2008 National Technical Meeting of The Institute of Navigation*, 2001. 911-922.

De Oliveira Moraes, A., De Paula, E. R., Perrella, W. J. & Da Silveira Rodrigues, F. 2013. On the distribution of GPS signal amplitudes during low-latitude ionospheric scintillation. *GPS solutions,* 17(4)**,** 499-510.

Elmas Z G, Aquino M, Forte B. The impact of ionospheric scintillation on the GNSS receiver signal tracking performance and measurement accuracy[C]// General Assembly and Scientific Symposium, 2011 XXXth URSI. IEEE, 2011:1-4.

Fortes, L. P. S., Lin, T. & Lachapelle, G. 2015. Effects of the 2012–2013 solar maximum on GNSS signals in Brazil. *GPS Solutions,* 19(2)**,** 309-319.

Fremouw, E. J., Leadabrand, R. L., Livingston, R. C., Cousins, M. D., Rino, C. L., Fair, B. C. & Long, R. A. 1978. Early results from the DNA Wideband satellite experiment—Complex‐signal scintillation. *Radio Science,* 13(1)**,** 167-187.

Huang, C. S., La, B. O., Roddy, P. A., Hunton, D. E., Liu, J. Y. & Chen, S. P. 2014. Occurrence probability and amplitude of equatorial ionospheric irregularities associated with plasma bubbles during low and moderate solar activities (2008–2012). *Journal of Geophysical Research Space Physics,* 119(2)**,** 1186-1199.

Humphreys, T. E., Psiaki, M. L. & Kintner Jr, P. M. 2010. Modeling the effects of ionospheric scintillation on GPS carrier phase tracking. *Aerospace and Electronic Systems, IEEE Transactions on,* 46(4)**,** 1624-1637.

Jiao Y, Yu M, Taylor S. Comparative studies of high-latitude and equatorial ionospheric scintillation characteristics of GPS signals[C]// Position, Location and Navigation Symposium - PLANS 2014, 2014 IEEE/ION. IEEE, 2014:37-42.

Jin, S., Feng, G. P. & Gleason, S. 2011. Remote sensing using GNSS signals: Current status and future directions. *Advances in Space Research,* 47(10)**,** 1645-1653.

Jin, S., Jin, R. & Kutoglu, H. 2016a. Positive and negative ionospheric responses to the March 2015 geomagnetic storm from BDS observations. *Journal of Geodesy*, 1-14.

Jin, S., Luo, O. F. & Park, P. 2008. GPS observations of the ionospheric F2-layer behavior during the 20th November 2003 geomagnetic storm over South Korea. *Journal of Geodesy,* 82(12)**,** 883-892.

Jin, S., Occhipinti, G. & Jin, R. 2015. GNSS ionospheric seismology: Recent observation evidences and characteristics. *Earth-Science Reviews,* 147**,** 54-64.

Jin, S., Rui, J. & Li, J. H. 2014. Pattern and evolution of seismo‐ionospheric disturbances following the 2011 Tohoku earthquakes from GPS observations. *Journal of Geophysical Research,* 119(9)**,** 7914-7927.

Jin, S. G., Jin, R. & Li, D. 2016b. Assessment of BeiDou differential code bias variations from multi-GNSS network observations. *Annales Geophysicae,* 34(2)**,** 259-269.

Kintner, P. M., Ledvina, B. M. & De, P. E. R. 2007. GPS and ionospheric scintillations. *Space Weather-the International Journal of Research & Applications,* 5(9)**,** 83-104.

Knight, M. F. 2000. Ionospheric scintillation effects on global positioning system receivers. *Doctoral dissertation,* The University of Adelaide.

Nunes F D, Sousa F M G. Practical simulation of GNSS signals in the presence of ionospheric scintillation[C]// IEEE/ION Position, Location & Navigation Symposium-plans. IEEE, 2014:50-58.

Oliveira Moraes, A., Paula, E. R. & Perrella, W. J. 2014. On the second order statistics for GPS ionospheric scintillation modeling. *Radio Science,* 49(2)**,** 94-105.

Prikryl, P., Jayachandran, P. T., Chadwick, R. & Kelly, T. D. 2015. Climatology of GPS phase scintillation at northern high latitudes for the period from 2008 to 2013. *Annales Geophysicae,* 33(5)**,** 531-545.

Tam Dao N H, Vinh Duong V. TEC and Scintillation observed over Ho Chi Minh, Vietnam during 2009-2012[C]// IEEE International Conference on Space Science and Communication. IEEE, 2013:434-439.

Wernik, A. W., Alfonsi, L. & Materassi, M. 2007. Scintillation modeling using in situ data. *Radio Science,* 42(1), RS 1002.

Yacoub, M. D. 2007. The alpha-mu Distribution: A Physical Fading Model for the Stacy Distribution. *IEEE Transactions on Vehicular Technology,* 56(1)**,** 27-34.

Yeh, K. C. & Liu, C.-H. 1982. Radio wave scintillations in the ionosphere. *Proceedings of the IEEE,* 70(4)**,** 324-360.